Research article

Giorgio Pettinari*, Loris Angelo Labbate, Mayank Shekhar Sharma, Silvia Rubini, Antonio Polimeni and Marco Felici

# Plasmon-assisted bandgap engineering in dilute nitrides

https://doi.org/10.1515/nanoph-2019-0025
Received January 28, 2019; revised March 15, 2019; accepted March 19, 2019

**Abstract:** The inherent ability of plasmonic bowtie nanoapertures (NAs) to localize the electromagnetic field at a subwavelength scale was exploited to engineer the H removal process in dilute nitrides at the nanometer level. Dilute nitride semiconductor alloys (e.g. GaAsN with a small percentage of nitrogen) are characterized by peculiar optoelectronic properties and, most importantly, by an even more peculiar response to hydrogen incorporation. In this class of materials, it is indeed possible to tune post-growth the alloy bandgap energy by a controlled incorporation of hydrogen atoms. The formation of N-H complexes neutralizes all the effects N has on the host matrix, among which is the strong narrowing of bandgap energy. In the present work, bowtie NAs resonant to the N-H complex dissociation energy were numerically modeled by finite element method simulations, realized by a lithographic approach, and characterized by scanning probe microscopy and resonant scattering spectroscopies. The conditions to get the maximum field enhancement at a specific position below the metal/semiconductor interface, namely at the dilute nitride quantum well position, were identified, demonstrating the ability to achieve a plasmon-assisted spatially selective hydrogen removal in a GaAsN/GaAs quantum well sample. Hydrogen removal through bowtie NAs turns out to be way more efficient (approximately two orders of magnitude) than through the plain surface, thus indicating that bandgap engineering through plasmonic nanostructures can be optimized for future efficient realization of site-controlled single-photon emitters and for their deterministic integration in plasmonic devices.

**Keywords:** plasmonics; bowtie nanoapertures; dilute nitrides; in-plane bandgap engineering; HSQ/PMMA lift-off.

## 1 Introduction

The study of plasmonic nanostructures continues to attract increasing interest, due to their potential application both in fundamental research and in device fabrication [1–3]. Among plasmonic nanostructures, nanoapertures (NAs) show the remarkable property to transmit and enhance the electromagnetic field over a subwavelength scale (i.e. well below the diffraction limit) [4–6]. This ability arises from collective excitations of the conduction electrons referred to as surface plasmon modes [7–10]. Having the ability to produce highly localized light spots, NAs can efficiently link propagating and localized optical fields, enhancing the interaction of light with matter at subwavelength resolution [11–13]. NAs could thus find potential applications in a number of fields where high optical resolution and field enhancement are critical, such as nanolithography [14–16], data storage [17], optical tweezers [18], or biochemical sensing [19–21]. In particular, given their geometry that merges both a high field enhancement due to plasmon coupling (feed-gap antenna effect) and a strong field localization due to the lighting rod effect [22], bowtie-shaped NAs are able to generate a very large field enhancement at their apexes [23], up to 15,000 times the illumination field [24].

In this work, we exploit the large field transmission and localization properties of bowtie NAs to directly write the bandgap energy of dilute nitrides, i.e. III-V semiconductor alloys containing small amounts of substitutional N atoms [25–27]. In previous works on the GaAsN alloy, to cite the most investigated dilute nitride material, we have

***Corresponding author: Giorgio Pettinari,** National Research Council (CNR), Institute for Photonics and Nanotechnologies (IFN-CNR), Via Cineto Romano 42, 00156 Roma, Italy, e-mail: giorgio.pettinari@cnr.it. https://orcid.org/0000-0003-0187-3770
**Loris Angelo Labbate:** National Research Council (CNR), Institute for Photonics and Nanotechnologies (IFN-CNR), Via Cineto Romano 42, 00156 Roma, Italy
**Mayank Shekhar Sharma, Antonio Polimeni and Marco Felici:** Physics Department, Sapienza University of Rome, P.le A. Moro 5, 00185 Roma, Italy
**Silvia Rubini:** National Research Council (CNR), Istituto Officina dei Materiali (IOM-CNR), S. S. 14, Km 163.5, 34149 Trieste, Italy

shown that it is possible to tune post-growth the alloy properties – e.g. the bandgap energy [28] or the effective mass [29, 30] and gyromagnetic factor [31] of conduction electrons – by a controlled incorporation of hydrogen atoms. This possibility stems from the formation of N-H complexes within the material lattice, which neutralize all the effects N has on the host matrix [32, 33]. More recently, we also demonstrated the possibility to modulate spatially, at a nanometer scale, the material properties, particularly the bandgap energy, by making use of lithographic [34] or laser-assisted [35, 36] approaches to control the incorporation or removal of hydrogen atoms, respectively. This ability has been successfully employed to create site-controlled quantum emitters and to deterministically integrate them in photonic crystal nanocavities [37, 38]. Here, by making use of plasmonic NAs, we engineer the plasmon-induced hot spot to control the N-H complex dissociation at the nanometer scale, opening a novel route to the hydrogen-induced in-plane bandgap engineering of dilute nitride semiconductors.

In particular, we perform finite element method (FEM) calculations (Section 2.1) to optimize the bowtie NA geometry in order to obtain a strong field localization (<100 nm) and enhancement (a factor of >10) 33 nm below the metal/semiconductor interface – namely, at the GaAsN quantum well (QW) center – for an incoming radiation wavelength of 700 nm. At that wavelength, indeed, the N-H complex dissociation by light has been reported to have the maximum efficiency [35]. Arrays of isolated bowtie NAs in Al thin films are then fabricated and characterized (Section 2.2) by scanning probe microscopies [i.e. scanning electron microscopy (SEM) and atomic force microscopy (AFM)] as a function of their geometrical properties. An electron beam lithography (EBL) fabrication approach is used, rather than the most widely used focused ion beam (FIB) milling approach, to keep the sample damage negligible during the fabrication of NAs and to allow a scalable processing of many devices in parallel over a relatively large area. The realized NAs are also experimentally characterized (Section 2.3) in terms of their optical response to the incoming radiation by cross-polarized resonant scattering spectroscopy, testing their resonant response to the target 700-nm radiation. Finally, the ability of the NAs to remove H in a spatially selective way from a fully hydrogenated GaAsN/GaAs QW sample is demonstrated (Section 3). The hydrogen removal through the NAs is way more efficient (up to ~100 times) than on the plain sample surface, thus demonstrating the potential of plasmon-induced in-plane bandgap engineering for the future efficient realization of site-controlled single-photon emitters in dilute nitrides and for their deterministic integration in plasmonic devices.

# 2 Bowtie NA optimization

Plasmonic NAs are characterized by a strong electromagnetic field localization and by a high transmission, which make them suitable for a variety of subwavelength applications. However, if not properly designed, the waveguide cut-off effect [39] can drastically reduce the field transmission through the plasmonic NA. For this reason, before fabrication, we have performed a series of FEM simulations, in order to define a range of geometric parameters suitable for the target application: namely, the site-controlled removal of H from a dilute nitride QW buried in a GaAs sample. In particular, the target bowtie NAs should be able to localize the field well below (33 nm) the metal/substrate interface, namely at the center of the QW, and they should sustain a plasmonic resonance at the near-infrared wavelength ($\lambda \sim 700$ nm) where the N-H complex dissociation and H removal from dilute nitrides are more efficient [35]. These are two stringent conditions specific to our target application and scarcely investigated in the literature.

## 2.1 Simulations

As the performance of a bowtie NA is strongly dependent on its geometry, in order to obtain reliable results when simulating the NA properties, it is necessary to adopt a realistic geometry, also taking into account the limits of the fabrication technique being used. Figure 1A shows the geometry of the bowtie apertures studied in this work. It consists of a square waveguide defined by a length $L$, loaded with two conducting triangular ridges whose apexes meet at the center of the aperture (initially no gap, $g = 0$). A square gap of size $g$ (≥10 nm, to meet the limit of the fabrication technique) is then opened at the center of the aperture. All the corners of the obtained geometry are rounded, with a minimum curvature radius of $r = 20$ nm, thus mimicking the finite resolution of the fabrication technique in the $xy$ plane while also avoiding field singularities in the simulations. The obtained bowtie geometry is used to define an aperture in a metal film of constant thickness ($t$) deposited on top of a GaAs substrate. The FEM simulation is then conducted by exciting such a geometry with a monochromatic plane wave of wavelength $\lambda$, linearly polarized with the electric field at a fixed angle ($\alpha$) with respect to the $y$-axis, originating from the air side and propagating at normal incidence with respect to the substrate. The simulations were performed for a range of wavelengths between 300 and 1100 nm. The refractive indices of the substrate (GaAs) and of the metal

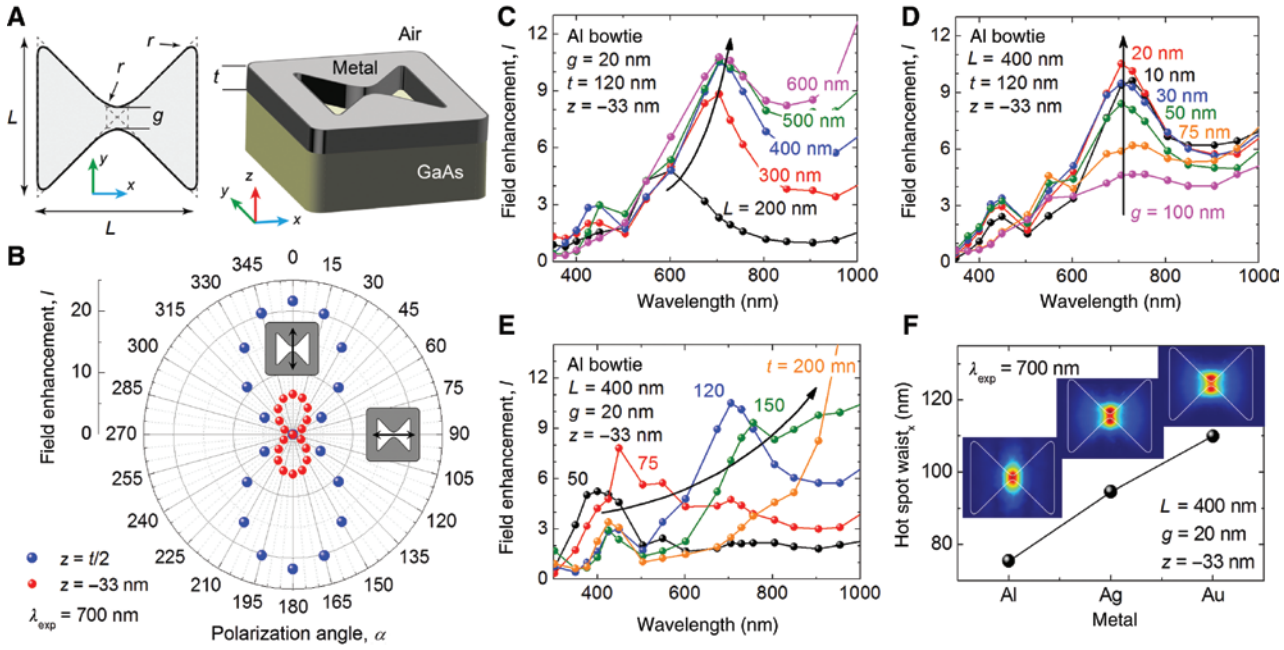


**Figure 1:** Bowtie NA simulations by FEM calculations.
(A) Geometry and 3D rendering of a bowtie NA. The outline dimension ($L$), gap size ($g$), minimum curvature radius ($r$), and metal thickness ($t$) are indicated in the figure, together with the $x$-$y$-$z$ axis orientation used throughout the paper. (B) Electromagnetic field enhancement ($I$; calculated as described in the text) produced by the bowtie NA at the gap center ($x=y=0$) for different values of $z$ (indicated in the figure; $z=0$ is set at the metal/substrate interface) as a function of the polarization direction of the incoming light ($\lambda_{exp}=700$ nm) and calculated for an aluminum bowtie NA on a GaAs substrate for $L=400$ nm, $g=r=20$ nm, and $t=120$ nm. The electromagnetic field enhancement at $z=-33$ nm as a function of the incoming radiation wavelength for different values of (C) outline dimension, (D) gap size, and (E) metal thickness has also been calculated for incoming light polarized along the $y$-axis; the parameters used in the calculations are given in the figure. (F) Hot-spot size along the bowtie main axis ($x$-axis) calculated at $z=-33$ nm for different metals (Al, Ag, Au). The FEM simulation maps of the electromagnetic field enhancement are reported as insets. The parameters used in the calculations are those maximizing the field enhancement for the specific metal ($t=80$ nm for Au and Ag; $t=120$ nm for Al).

layer used for the NA were wavelength dependent and were interpolated based on empirical data [40, 41], while a wavelength-independent refractive index of 1.0 was used for the environment (air). The computational domain box had a size of 1500 nm with a perfectly matched layer of 150 nm around it[1]. A finer mesh (5–7 nm) was used around the NA, while a coarser mesh (50–80 nm) was employed in the outer regions. A perfect electric conductor was used in the $y$-$z$ and $x$-$z$ edge planes. The simulations were performed by calculating first a background scattered field ($E_0$), defined as the solution of the interaction between the plane wave and an infinite metallic slab without any aperture (Floquet periodic boundary conditions were used in this case). Such an $E_0$ field was then used as the excitation field for a second calculation run, where a single bowtie NA was opened in the metallic slab. The total electric field ($E_{tot}$) obtained in such a way can be seen as the superposition of the background field produced by the metallic slab and the scattered field ($E_{NA}$) produced by the NA: $E_{tot}=E_0+E_{NA}$. Finally, the field intensity enhancement ($I$) produced by the single NA was obtained for each point of the simulated three-dimensional (3D) space as the ratio between the square norm of the total field and the square norm of the background field: $I=||E_{tot}||^2/||E_0||^2$. Such a simulation strategy yields accurate results even in the case $E_{NA} \ll E_0$ and does not require a strong calculation power, as it can be performed on a desktop (32 Gb RAM) computer; however, it is a bit more time consuming, as any simulation has to be performed twice (with and without the NA) for each geometry and incident radiation condition.

As widely reported in the literature [23, 42, 43], the spectral response of metallic bowtie NAs is dominated by a surface plasmon resonance at visible/far-infrared

**1** The role of the box size of the computational domain has been checked by preliminary simulations with different box sizes, as well as by reproducing published results obtained by different groups employing different simulation setups. The very localized nature of the scattered fields in the plasmonic NAs makes it possible to keep the computational domain rather small, without introducing simulation artifacts.

wavelengths and by a Fabry-Pérot-like resonance at visible/ultraviolet wavelengths. By varying the NA geometry, mainly the film thickness, the relative intensity of the two resonances can be varied and one resonance can be enhanced with respect to the other. Figure 1 summarizes the results of the simulation studies done by varying all the geometrical parameters of the NA (i.e. outline dimension $L$, gap size $g$, metal thickness $t$, and the type of metal employed). The final goal of this study was to maximize the field intensity and localization (i.e. hot-spot lateral size) at the QW position (33 nm below the metal/substrate interface) for an incoming radiation of 700-nm wavelength. As a general trend, and in agreement with the literature [23, 24, 42, 44, 45], we found that an efficient plasmon resonance excitation can be achieved only for incoming light linearly polarized orthogonal to the bowtie main axis (i.e. along the $y$-axis), while surface plasmons are not excited for polarization along the bowtie main axis (i.e. $x$-axis). Such a polarization dependence is retained by the radiation transmitted through the NA toward the substrate (see Figure 1B). The field enhancement and resonant wavelength values are then analyzed adopting the convenient polarization for the incoming light (i.e. along the $y$-axis). We found that the field enhancement increases for decreasing the gap size from 100 to 10 nm, exhibiting a rather flat maximum around $g \sim 20$ nm (Figure 1D), and that the intensity increases and the resonance frequency redshifts for increasing the outline dimensions from 200 to 600 nm, saturating for $L \geq 400$ nm (Figure 1C). Finally, a strong dependence of the plasmonic peak, both in intensity and resonant wavelength, is found by varying the metal thickness (see Figure 1E). Fixing all the geometrical parameters to the values that produce the strongest resonance peak for an incoming radiation of 700-nm wavelength, we investigated the different metals usually employed in plasmonics – such as gold, silver, and aluminum – looking for the minimum hot-spot size that can be produced at the QW level ($z = -33$ nm). Although Au and Ag are able to produce a stronger field intensity enhancement (about three times that produced by Al), Al guarantees the most localized hot spot among the three metals, as well as the most symmetric one (see Figure 1F).

The performed simulation study allows us to identify the parameters a bowtie NA should have to produce an efficient H removal from a dilute nitride QW sample, which turn out to be $L = 400–600$ nm, $g = 20–50$ nm, $t = 100–120$ nm in an Al film. This defines relatively lax conditions on the bowtie geometry, such that even relatively large variations in the geometric properties of the fabricated NAs (up to 20% around the optimal value of $L$ and $t$, and up to 40% for $g$) are not expected to sizably worsen (<20%) the hot-spot intensity generated by the NA. Moreover, the use of Al (instead of Au or Ag) as the metal employed for making the NAs contributes to keeping the process cheap, which, paired to an inherently scalable fabrication technique (see below), greatly enhances the potential for applications of the results presented here.

## 2.2 Fabrication

The possibility to realize plasmonic nanostructures with gap size <10 nm has been demonstrated for different fabrication approaches: angled deposition [46], self-assembly of nanoparticles [47], chromium expansion with a second lithography [48], and template stripping from a silicon substrate [49, 50]. Nevertheless, FIB milling is still the most used technique to achieve narrow-gap plasmonic aperture devices [51], having shown the capability to produce – with an $He^+$-ion lithography configuration – apertures with gap size down to 8 nm in coaxial shapes [52] and 5 nm in dimers [53–55]. Although FIB-based fabrication techniques allow ultimate gap resolution, they are often very challenging, not scalable, and not very versatile. Moreover, they are serial in nature, and thus unsuited for the fabrication of large arrays of devices. On the contrary, EBL – possibly combined with a single lift-off step to produce the final structure – is a much more flexible technique, naturally suited to be scalable and capable of producing high-resolution features at a much higher production rate. In this study, we adopted one such EBL-based fabrication technique by optimizing a negative-tone lift-off process with a hydrogen silsesquioxane/poly(methylmethacrylate) (HSQ/PMMA) bilayer resist for the realization of plasmonic NAs. A lithographic approach followed by a modified lift-off process has recently shown the ability to fabricate 10-nm-gap bowtie NAs [56]. However, in that case, a single-layer HSQ resist was employed paired with a lift-off performed in hydrofluoric acid, which is not suitable for all substrates nor is it compatible with Al films. Here, to avoid hydrofluoric acid as the remover, an HSQ/PMMA bilayer resist was employed, thus allowing to remove the resist in an organic solvent (i.e. acetone). The negative-tone lift-off process with the HSQ/PMMA bilayer resists has already been proposed in the literature [57], with a reported sub-10-nm resolution [58]; however, to the best of our knowledge, it has never been applied to the fabrication of plasmonic nanostructures.

The fabrication procedure used is outlined in Figure 2. Our devices are fabricated on epitaxial GaAs samples

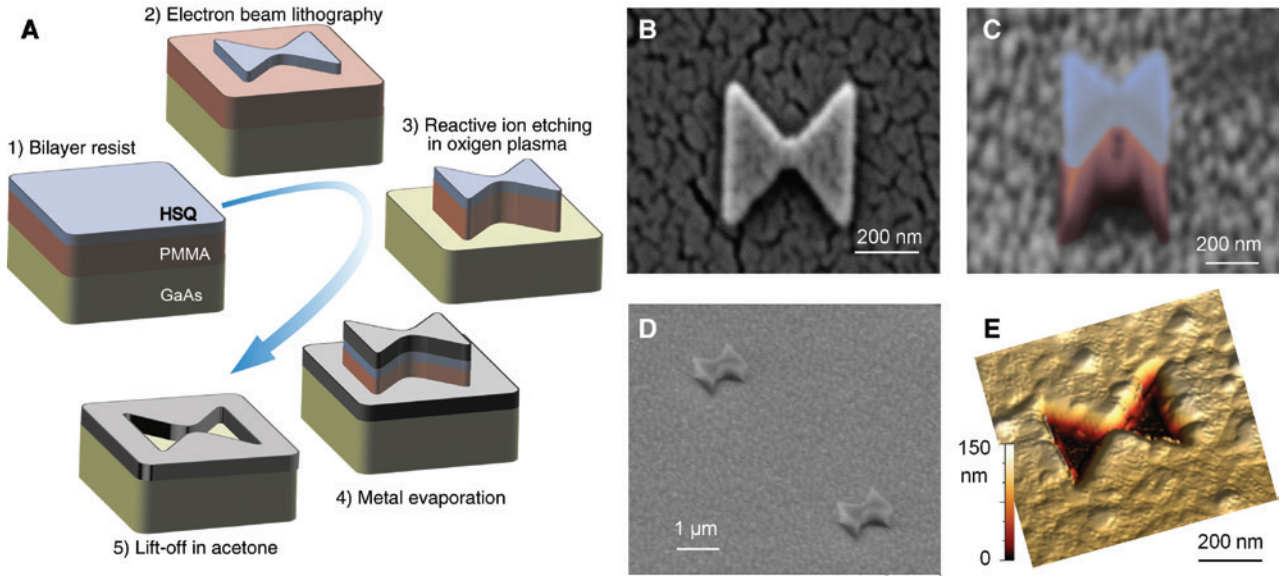


**Figure 2:** Bowtie NA fabrication.
(A) Sketch of the processing steps leading to the fabrication of metal bowtie NAs by a negative-tone lift-off process employing the EBL of an HSQ/PMMA bilayer resist. SEM images of the sample (B) after the patterning of the top HSQ layer (step 2), (C) after the patterning of the HSQ/PMMA layers (52° tilted image; false colors highlight the 70-nm-thick HSQ layer on top of the 300-nm-thick PMMA one; step 3), and (D) after the metal deposition (45° tilted image; step 4). In panel (B), a thin Au layer has been deposited on the sample surface to mitigate the charging effects during the SEM acquisition. (E) AFM map of a final structure (Al on GaAs, $L = 400$ nm, $g = 30$ nm, $t = 120$ nm).

(with and without the presence of a buried GaAsN QW; see Figure 2A for a sketch of the whole processing chain). First, a positive-tone PMMA electron resist is spin-coated on the sample, forming a 300-nm-thick resist film on top of which a second layer of negative-tone HSQ electron resist is deposited with a thickness of 70 nm. An EBL system (VISTEC EBPG 5-HR working at 100 kV) is used to pattern bowtie shapes with an *e*-beam dosage ranging from 1300 to 1900 µC/cm$^2$, depending on the feature size. After the exposure, HSQ is developed at 20°C in an aqueous solution of tetramethylammonium hydroxide at 2.4% for 60 s, and then backed on a hot plate at 130°C for 5 min to increase the chemical and physical stability of the HSQ to the subsequent processing steps (Figure 2B). The bowtie shapes are then transferred to the PMMA layer by reactive ion etching in an $O_2$:Ar (3:1) gas mixture plasma, thus leaving behind tall (~370 nm) bowtie posts (see Figure 2C). The presence of $Ar^+$ ions in the plasma helps to reach near perpendicular sidewalls in the HSQ layer and a pronounced undercut in the PMMA layer, both conditions extremely important to prevent sidewall coating during the metal deposition (Figure 2D) and, thereby, to allow for a high-quality lift-off even with a rather small resist-to-metal ratio (3:1 in our case). Any possible oxidation of the sample surface and/or PMMA residuals is removed just before the metal deposition by a further mild reactive ion etching step in $CHF_3$ plasma. Next, a 120-nm-thick layer of aluminum is evaporated onto the sample, and the final lift-off is performed in hot acetone (56°C) in a sonication bath cleaner for 2 min.

In the fabrication protocol, each step has been carefully optimized to control the final feature sizes and metal roughness; in particular, the etching steps are those most critical in this respect. As discussed in the next section, the metal roughness strongly affects the plasmon resonance in a way hard to quantify by simulations, so a fabrication strategy able to control such a parameter is instrumental to get efficient, reproducible plasmonic structures. The developed fabrication protocol allows for the realization of large arrays of (thousands of) identical bowtie NAs with outline dimension ($L$) down to 200 nm, gap size ($g$) down to ~30 nm, in an Al film ($t = 120$ nm) having a root mean squared (Rms) surface roughness as low as 1.1 nm (see Figure 2E).

## 2.3 Optical characterization

The optical properties of the fabricated bowtie NAs, in particular their ability to enhance the intensity of an incoming electromagnetic radiation at the plasmon resonance wavelength, have been tested by resonant scattering spectroscopy performed in a cross-polarization configuration [59, 60]. In such a configuration, a laser light linearly

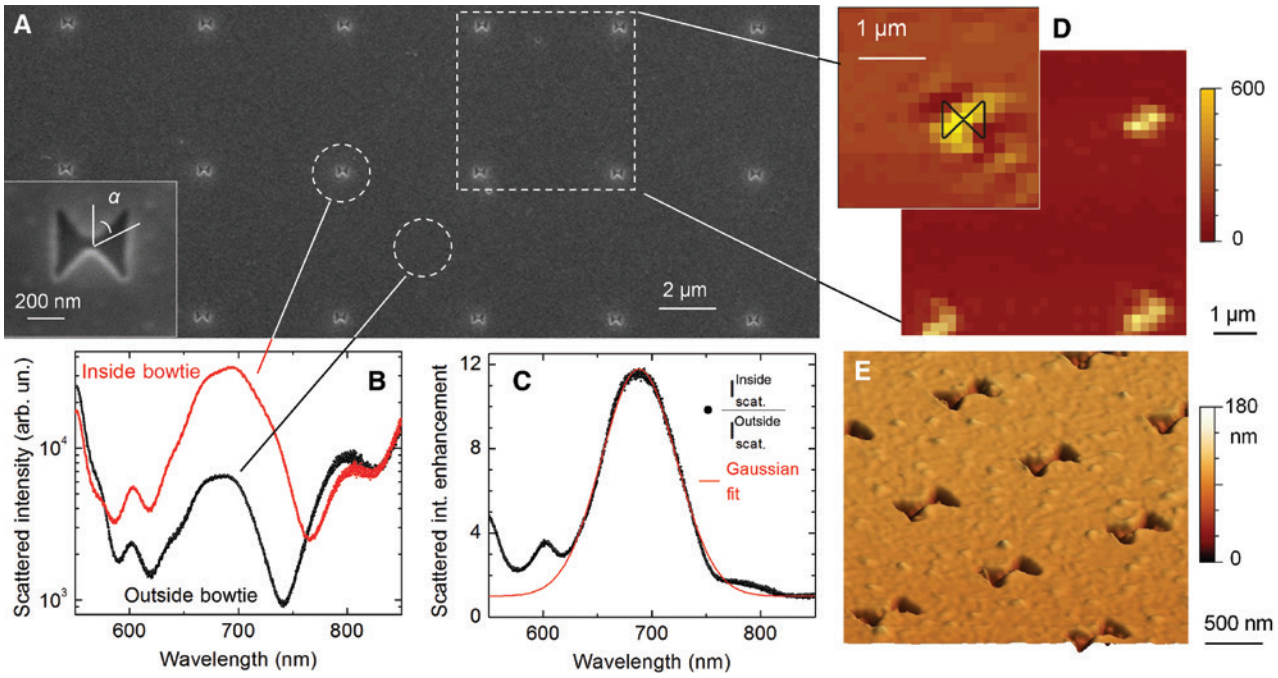


**Figure 3:** Bowtie NA characterization.
(A) SEM image of an array of bowtie NAs fabricated in a 120-nm-thick aluminum layer on top of a GaAs sample ($L = 400$ nm, $g = 50$ nm, array pitch of 5 μm); a zoom of a single structure is given in the inset where the polarization angle ($\alpha$) for the incoming radiation is also indicated. (B) The resonant scattering spectra acquired on a single bowtie (red points) and on the unpatterned Al layer (black points) are used to calculate the (C) scattered intensity enhancement produced by the bowtie aperture. A Gaussian resonance centered at $\lambda \sim 700$ nm is found, in agreement with the simulations reported in Figure 1D. (D) Map of the resonant scattering enhancement integrated around 700 nm (over a 50-nm interval) acquired on a $7 \times 7$ μm$^2$ area. The inset shows the map of a single bowtie (sketched in black on top of the map) where it is possible to distinguish two darker regions around a bright spot. This can be associated to the plasmon-induced localization of the scattered field, which is collected from the bowtie arms and concentrated into the bowtie gap. The inclination at ~45° of the scattered intensity from the bowtie is the result of the cross-polarization scheme ($\alpha = 45°$) used for the measurements (see also text and Figure 4G). (E) AFM map of an array of bowtie NAs similar to that shown in panel (A) but with an array pitch of 1 μm.

polarized at an angle $\alpha$ with respect to the bowtie $y$-axis (see inset in Figure 3A) is sent to the sample through a microscope objective. The light scattered from the sample is then collected by the same objective, in a cross-polarization scheme (i.e. selecting only the light linearly polarized at $\alpha + 90°$). This technique efficiently removes the reflected light coming from the sample surface, thus enhancing the sensitivity to the scattered light. A confocal Raman microscope equipped with a 100× objective (with a numerical aperture of 0.9) was employed to reach a laser spot size of ~0.6 μm at the sample surface, thus allowing us to investigate the response of a single NA (the NA-NA spacing was ≥1 μm in the fabricated arrays; see Figure 3A,E). The incident light was provided by a supercontinuum laser source with wavelengths ranging from ~480 to ~2400 nm, then selected and linearly polarized in the range 480–1000 nm by a combination of a 1000-nm short-pass filter, a 435-nm long-pass filter, and a linear polarizer. Meanwhile, the collected light was polarization-rotated by a half-wave plate and filtered by a polarizer set (i) at 90° with respect to the polarization of the incident light and (ii) aligned with the direction of the maximum response of the detection system. Finally, the signal was analyzed by a spectrometer equipped with a 300 groove/mm grating and an Si charge coupled device detector. The spectrum of the scattered light intensity produced by the NA is obtained by normalizing the scattered light measured from the NA to that measured on an unpatterned area of the same metal film, which automatically rids us of the wavelength dependence of the incident radiation intensity and of the response of the optical elements (see Figure 3A–C). A Gaussian profile centered at the target wavelength of 700 nm is found for all the investigated NAs (i.e. Al bowties with $L = 300–600$ nm, $g = 30–70$ nm, and $t = 120$ nm; see also Figure 4D), thus validating the simulation studies and the fabrication protocol.

The ability of EBL to easily create arrays of identical objects on a large area is evident by the optical and surface probe microscopy (SEM and AFM) maps acquired on the realized samples (see Figure 3A,D,E).

A 2D map of the scattered light intensity integrated around 700 nm is reported in Figure 3D. Although the spatial resolution of the map (limited by the laser spot size of ~0.6 μm) is comparable with the size of the investigated NA, and so a map of the plasmonic mode itself is not possible, it is possible to envisage two darker regions around a bright spot centered on the bowtie aperture. We tentatively attribute this feature to the plasmon-induced localization of the scattered field, which is collected from the bowtie arms and concentrated into the bowtie gap. Maps at higher spatial resolution, as those obtainable by near-field spectroscopy (planned for the near future), could validate or reject this hypothesis.

One of the advantages of the chosen fabrication strategy was to have a direct, easy control on the metal surface roughness. It was possible, indeed, to fabricate identical bowtie NAs with metal surface roughness varying over more than an order of magnitude (i.e. Rms from 1.1 to 18.7 nm) by changing the etch recipe, thus directly testing the metal roughness effect on the plasmon resonance by measuring the optical response of the different NAs. Metal surface roughness is known to play a crucial role in plasmonics, as it is one of the main parameters affecting the plasmon excitation time dephasing and damping mechanics [61]. Its effects are usually detrimental for the properties of the plasmonic nanostructures, particularly in the far-field configuration, even if they can have advantages on the near-field properties, as those reported in surface-enhanced Raman spectroscopy experiments [62]. Nevertheless, surface roughness effects are difficult to model and can often be addressed only through direct measurements. In Figure 4A–C, we report an optical and structural investigation of identical bowtie NAs in a 120-nm-thick Al film ($L = 600$ nm, $g = 35$ nm) with very different metal surface roughness (as measured by AFM). By increasing the surface roughness, the scattered intensity enhancement peak shifts to higher wavelengths, broadens, and loses in intensity, all but vanishing for the sample with the highest roughness (Rms = 18.7 nm). Such a behavior agrees with what is reported in the literature for plasmonic gold nanoshells, as a result of the roughness-induced plasmon damping and "hot-spot" formation

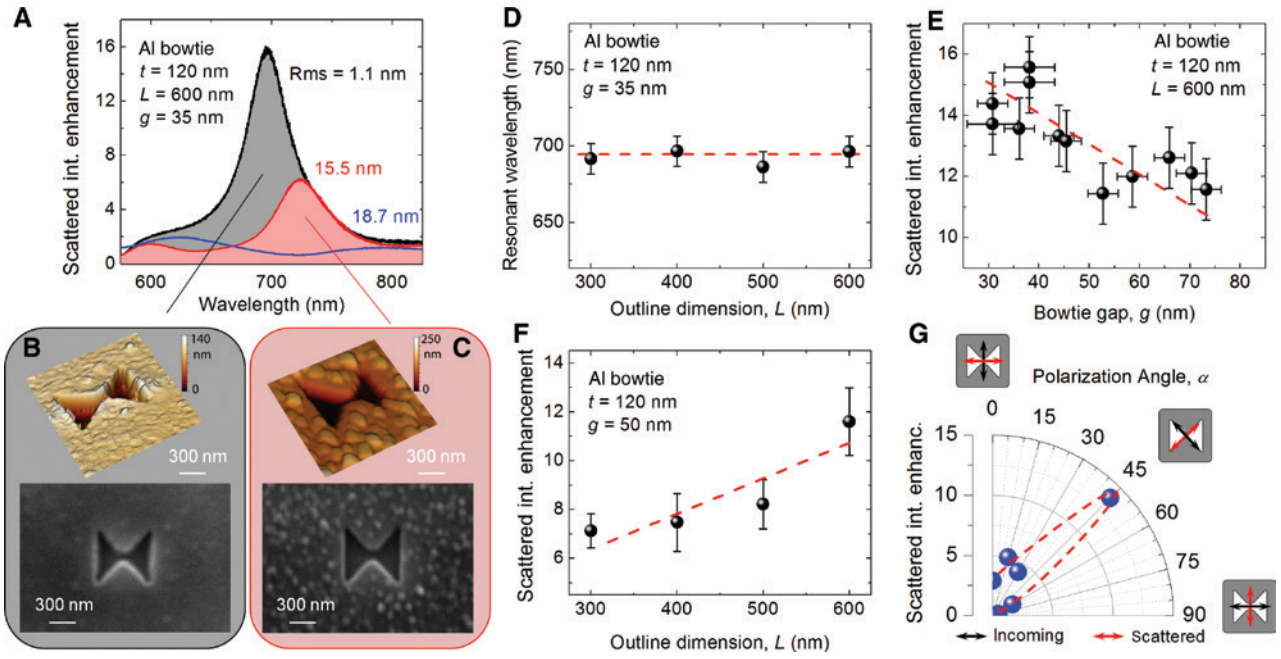


**Figure 4:** Bowtie NA optical properties.
(A) Scattered intensity enhancement spectrum for a same Al bowtie NA geometry with different values of metal surface roughness (Rms from 1.1 to 18.7 nm). By increasing the metal surface roughness, the plasmonic peak shifts to higher wavelengths, broadens, and loses in intensity, all but disappearing for the roughest sample. SEM and AFM maps for two representative NAs are reported in panels (B) and (C). The values obtained for the smoother sample for (D) the resonant wavelength as a function of bowtie outline dimension, and for the scattered intensity maximum enhancement as a function of (E) gap size or (F) outline dimension, are also given. (G) Scattered intensity maximum enhancement as a function of the polarization angle (as acquired on a bowtie NA having $L = 400$ nm, $g = 30$ nm, $t = 120$ nm). The maximum enhancement is obtained for a 45° polarization, as a consequence of the plasmon excitation dependence on the incoming radiation polarization (see Figure 1B) and the cross-polarization scheme employed for the measurements. Dashed lines are guide to the eye. Note that all experimental trends of the optical properties of the realized bowtie NAs are in agreement with the predictions of the FEM simulations given in Figure 1.

on the surface corrugations [61, 62]. For our purposes, being interested in getting the strongest far-field enhancement from the bowtie NAs, in the fabrication process optimization we gave priority to a process leading to smooth metal surfaces, somewhat sacrificing the achievement of ultimately high gap resolution. The actual feature sizes of the fabricated NAs have been determined by surface probe microscopes (SEM and AFM); gap sizes down to 30 nm have been obtained in samples showing very small surface roughness (Rms ~ 1 nm). On such samples characterized by a smooth surface, we investigated the dependence of the scattering intensity enhancement as a function of the bowtie outline dimension and gap. As regards the scattered field enhancement, we found that it increases both by decreasing the gap size (Figure 4E) and by increasing the NA outline dimension (Figure 4F). These behaviors agree well with what is expected on the basis of the performed simulations. Moreover, we investigated the optical response as a function of the polarization angle of the incoming radiation for an NA with $L = 400$ nm and $g = 30$ nm (see Figure 4G). We found an almost vanishing value of the field enhancement for $\alpha = 0°$ (polarization of the incoming light along the *x*-axis), a rather small value (~3) for $\alpha = 90°$[2], and a marked maximum (~14) for $\alpha = 45°$. Also, this experimental behavior perfectly agrees with the expectations (see Figure 1B) once the cross-polarization configuration employed in the measurements is duly considered. Indeed, when the polarization of the incoming light is along the *x*-axis, the surface plasmon excitation is negligible. On the contrary, for polarization along the *y*-axis, the plasmon is maximally excited. However, in this configuration, the scattered light (also polarized along the *y*-axis) is cut by the collection polarization (fixed along the *x*-axis)[2]; thus, the maximum intensity is found for $\alpha = 45°$.

## 3 Plasmon-assisted H removal

As mentioned in Section 1, the spatially controlled, post-growth incorporation or removal of hydrogen in dilute nitride semiconductors can be applied to the fabrication of site-controlled quantum dots (QDs) [34, 36]. In particular, as regards H removal, a near-field optical illumination was recently employed to overcome the wavelength diffraction limit, thus reducing the laser-irradiated area down to a size of <100 nm and inducing quantum confinement effects [36]. The ability of plasmonic NAs to localize the electromagnetic field at a subwavelength level may make it possible to obtain similar results simply by illuminating the sample through a standard microscope objective, thus avoiding the need for a complex near-field illumination setup. To this end, we first test and demonstrate the possibility to obtain a controlled H removal, and the ensuing in-plane modulation of the bandgap of dilute nitrides, through plasmonic NAs. Figure 5A shows a sketch of the experiment we performed. We studied a GaAs sample containing a GaAsN QW ([N] = 1.1%) buried 30 nm below the surface of the sample, which was hydrogenated (H-dose equals to $1.5 \times 10^{17}$ ions/cm$^2$, hydrogenation temperature equals to 190°C) in such a way to get a complete N passivation. The achievement of this condition is confirmed by the photoluminescence (PL) spectrum of the sample after hydrogenation, in which only the GaAs emission can be detected (see black line in Figure 5B). After H irradiation, an array of identical Al bowtie NAs was fabricated on the sample following the procedure described in Section 2.2 ($t = 120$ nm, $L = 600$ nm, $g = 100$ nm, array pitch of 5 μm). Then, laser exposures via a 50× microscope objective (numerical aperture of 0.5, laser spot size ~1.7 μm) were performed on single bowtie NAs by shining a 100-nm band laser centered at $\lambda_{exp} = 700$ nm (as obtained from a supercontinuum laser with the aid of optical filters). The laser treatments were performed for a fixed exposure time of 1 s at increasing power densities. The H removal efficiency was tested by measuring the room temperature PL spectrum from the single NAs after each laser treatment. The PL was excited with a 532-nm laser operated at a power (<1 mW) sufficient to generate a sizable PL signal without producing any H removal (in this, we were aided by the fact that in GaAsN, the H-removal efficiency at 532 nm is about four times lower than that at 700 nm [35]).

For laser treatments performed at a power of >1 mW, it was possible to observe a sizable hydrogen removal, as indicated by the appearance of the GaAsN peak in the PL spectrum, with a relative intensity increasing as a function of the laser power used in the treatment (see Figure 5B, red and blue lines). It is worth mentioning that the laser power necessary for a full dehydrogenation of the GaAsN QW through the bowtie NA (i.e. 6 mW for 1 s, for a GaAsN emission energy matching the one of the hydrogen-free sample) is seemingly unable to remove any H from the unpatterned area of the same sample (see inset in Figure 5B). As extensively detailed in previous studies on similar samples, indeed, a laser treatment at a power higher than ~30 mW for 20 s is necessary in order to produce a full de-hydrogenation on unpatterned samples [35]. The reported results indicate, therefore, that

**2** The presence of a non-vanishing scattered intensity enhancement for an incoming polarization angle $\alpha = 0°$ can be due either to a not perfect extinction ratio of the cross-polarization configuration, to a partial depolarization of the scattered light, or to both of them.

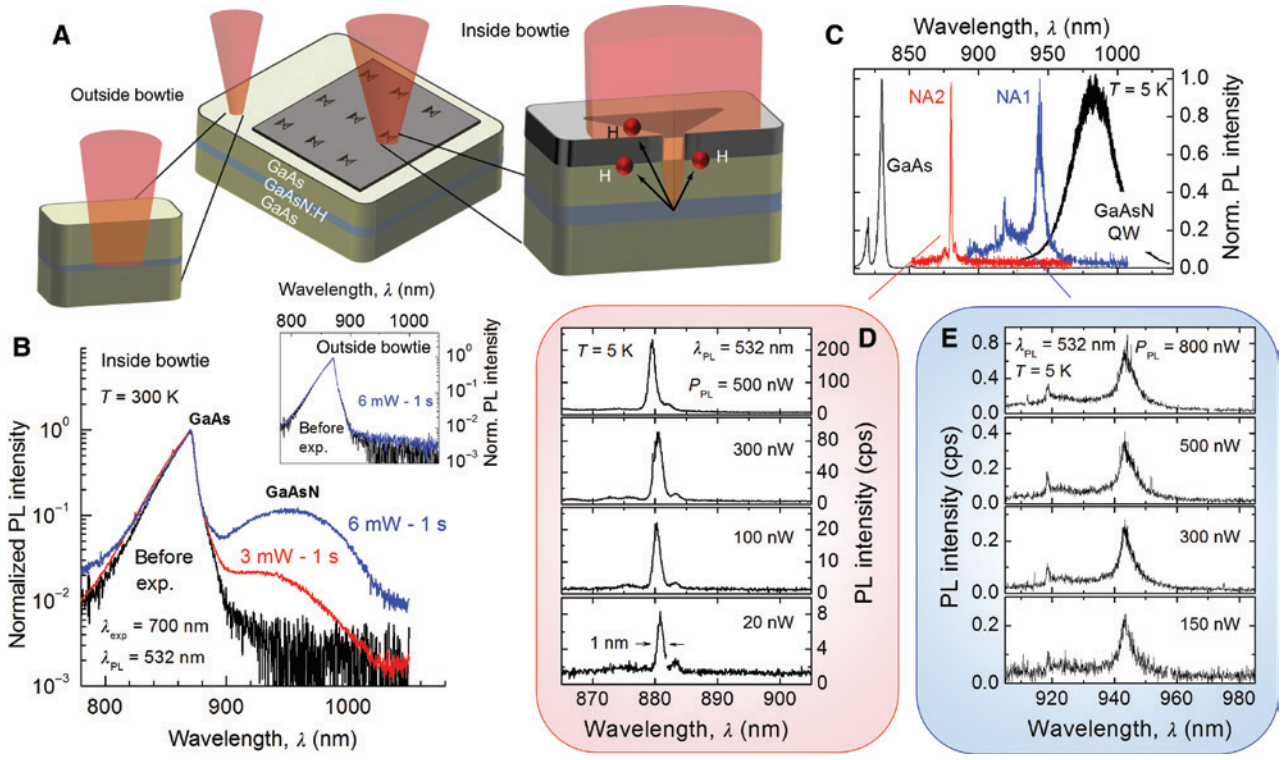


**Figure 5:** Plasmon-assisted H removal in dilute nitrides.
(A) Sketch of the plasmon-assisted H removal in a fully hydrogenated GaAsN/GaAs QW sample patterned with bowtie NAs. An array of bowtie NAs ($L = 600$ nm, $g = 100$ nm, array pitch of 5 μm) is fabricated in a 120-nm-thick aluminum layer on top of a fully hydrogenated ($d_H = 1.5 \times 10^{17}$ ions/cm$^2$) GaAs sample containing a 6-nm-thick GaAsN QW buried 30 nm below the sample surface. Laser exposures ($\lambda_{exp} = 700$ nm) of 1 s at different power levels are performed through single bowtie NAs in order to remove H in a spatially selective way. (B) The H removal efficiency is tested by PL investigation of the NAs after the laser treatment exposures. The same treatments are performed also on unpatterned areas for comparison purposes (see inset). The H removal through the bowtie NA is complete for a treatment at 6 mW for 1 s, a condition that does not produce any sizable effect on the unpatterned region. (C) Low temperature ($T = 5$ K) PL spectra acquired on two NAs after laser treatments at different conditions (blue line: 6 mW for 1 s; red line: 2 mW for 3 s). The spectra of the GaAs substrate and of the hydrogen-free QW (black lines) are also reported for comparison purposes. PL power-density studies are also reported in panels (D) and (E).

the H removal process through the NA is much more efficient (~100 times, when the amount of energy delivered to the sample by the laser is considered) than on the plain surface, and that the plasmon-induced hot spot created by the bowtie NA in correspondence of the GaAsN QW level is able to produce an in-plane bandgap engineering modulation.

Moreover, the simulations indicate that, by reducing the bowtie NA gap to <50 nm, the hot spot created at the GaAsN QW level is localized on a lateral size <100 nm (see Figure 1F, for $g = 20$ nm). As a consequence, we expect to be able to exploit such a plasmon-enhanced H removal to create nanostructures (such as QDs) by illuminating bowtie NAs through a standard microscope objective, in a similar (but much simpler) way to what is done by near-field optical illumination [36]. Low-temperature measurements on NAs treated under specific irradiation conditions indeed show the presence of narrow lines (with full-width-half-maximum down to ~1 nm) peaked at energies higher than that of the pristine GaAsN QW ($\lambda \sim 980$ nm at $T = 5$ K), which may indicate the formation of a GaAsN QD within the treated area (see Figure 5C–E). In particular, it is worth noticing that delivering a same amount of energy (6 mJ) through identical NAs ($L = 400$ nm, $g = 100$ nm) but employing different power and treatment times (e.g. 6 mW for 1 s, or 2 mW for 3 s; see blue and red lines in Figure 5C, respectively), the formed nanostructures can exhibit very different emission energies (up to ~100 meV apart each other). This seems to suggest that the actual size of the GaAsN nanostructure created by NAs is not only defined by the NA geometry, but can also be tuned by the laser treatment parameters, similar to what is found in the case of near-field illumination [36]. A detailed investigation on the QD formation by plasmon-assisted H removal is under progress and will be reported elsewhere.

## 4 Outlook and conclusion

In summary, bowtie-shaped plasmonic NAs have been investigated and fully optimized, opening a new pathway to the efficient in-plane bandgap engineering of hydrogenated dilute nitrides by spatially selective H removal. Bowtie NAs resonant to the N-H complex dissociation energy ($\lambda \sim 700$ nm) have been numerically modeled by FEM simulations, realized by a lithographic approach avoiding the use of focused ion milling, and characterized by scanning probe microscopy and resonant scattering spectroscopies. The conditions to get the maximum field enhancement at a specific position below the metal/semiconductor interface (namely, at the center of the dilute nitride QW) have been identified, and we demonstrated the achievement of plasmon-assisted spatially selective hydrogen removal in a fully hydrogenated GaAsN/GaAs QW sample. Hydrogen removal through bowtie NAs turns out to be two orders of magnitude more efficient than through the plain surface of the sample. Ordered arrays of identical Al bowtie NAs have been fabricated by *e*-beam lithography, followed by a single lift-off step. In spite of its simplicity, this method can be employed to shape a wide range of complex nanostructure designs with good resolution and reproducibility, without involving aggressive etching processes or damaging focused ion milling steps. In addition, the roughness of the metal film, which has been shown to strongly affect the plasmon resonance condition, can be controlled by varying the process parameters and can be kept at a very low level (as low as Rms ~ 1 nm).

The reported findings demonstrate that bandgap engineering through plasmonic nanostructures represents a versatile and powerful tool to control the optoelectronic properties of dilute nitrides in a spatially controlled way. In particular, the reported study represent a first, pivotal step toward the realization of deterministically coupled optically active semiconductor-plasmonic integrated components, of great interest for the practical implementation of quantum information and communication protocols [63]. Indeed, the demonstrated ability to locally manipulate the bandgap energy of hydrogenated dilute nitrides via plasmonic NAs can lead to the realization of spatially controlled QDs, which can be directly coupled with the plasmonic nanostructures used to fabricate them. Ideally, it might even be possible to purposely design doubly resonant plasmonic structures [64], with one resonance centered at 700 nm – to have efficient H removal to create the QD – and the other resonance peaked at ~900 nm – to boost and control the emission properties of the fabricated nanostructures.

**Acknowledgment:** This work was supported by the Italian Ministry for Education, University and Research within the Futuro in Ricerca (FIRB) program (project DeLIGHTeD, Prot. n. RBFR12RS1W, Funder Id: http://dx.doi.org/10.13039/501100003407) and by the European Union's Horizon 2020 Research and Innovation Program under the Marie Skłodowska-Curie Grant Agreement No. 641899 PROMIS (Postgraduate Research on Dilute Metamorphic Nanostructures and Metamaterials in Semiconductor Photonics), Funder Id: http://dx.doi.org/10.13039/100010665. A.P. and M.F. acknowledge funding from the Regione Lazio programme "Progetti di Gruppi di ricerca" legge Regionale n. 13/2008 (SINFONIA project, prot. n. 85-2017-15200) via LazioInnova spa.

## References

[1] Greffet J-J. Nanoantennas for light emission. Science 2005;308:1561–3.
[2] Mühlschlegel P, Eisler H-J, Martin O, Hecht B, Pohl D. Resonant optical antennas. Science 2005;308:1607–9.
[3] Ozbay E. Plasmonics: merging photonics and electronics at nanoscale dimensions. Science 2006;311:189–93.
[4] Ebbesen TW, Lezec HJ, Ghaemi HF, Thio T, Wolff PA. Extraordinary optical transmission through sub-wavelength hole arrays. Nature 1998;391:667–9.
[5] Garcia-Vidal FJ, Moreno E, Porto JA, Martin-Moreno L. Transmission of light through a single rectangular hole. Phys Rev Lett 2005;95:103901.
[6] Thio T, Pellerin KM, Linke RA, Lezec HJ, Ebbesen TW. Enhanced light transmission through a single subwavelength aperture. Opt Lett 2011;26:1972–4.
[7] Barnes WL, Dereux A, Ebbesen TW. Surface plasmon subwavelength optics. Nature 2003;424:824–30.
[8] Genet C, Ebbesen TW. Light in tiny holes. Nature 2007;445:39–46.
[9] White JS, Veronis G, Yu Z, et al. Extraordinary optical absorption through subwavelength slits. Optics Lett 2009;34:5.
[10] Stockman M. Nanoplasmonics: the physics behind the applications. Physics Today 2011;64:39.
[11] Schuller JA, Barnard ES, Cai W, Jun YC, White JS, Brongersma ML. Plasmonics for extreme light concentration. Nat Mater 2010;9:193–204.
[12] Gramotnev DK, Bozhevolnyi SI. Plasmonics beyond the diffraction limit. Nat Photon 2010;4:83–91.
[13] Biagioni P, Huang JS, Hecht B. Nanoantennas for visible and infrared radiation. Rep Prog Phys Phys Soc 2012;75:024402.
[14] Wang L, Uppuluri SM, Jin EX, Xu X. Nanolithography using high transmission nanoscale bowtie apertures. Nano Lett 2006;6:361–4.
[15] Wen X, Datta A, Traverso LM, Srisungsitthisunti P, Xu X, Moon EE. Optical nanolithography with $\lambda/15$ resolution using bowtie aperture array. Appl Phys A 2014;117:307–11.
[16] Wen X, Traverso LM, Pan L, Xu X, Moon EE. High throughput optical lithography by scanning a massive array of bowtie aperture antennas at near-field. Sci Rep 2015;5:16192.

[17] Peng C, Jin E, Clinton TW, Seigler MA. Cutoff wavelength of ridge waveguide near field transducer for disk data storage. Opt Express 2008;16:16043–51.
[18] Berthelot J, Aćimović SS, Juan ML, Kreuzer MP, Renger J, Quidant R. Three-dimensional manipulation with scanning near-field optical nanotweezers. Nat Nanotechnol 2014;9:295–9.
[19] Fromm DP, Sundaramurthy A, Kinkhabwala A, Schuck PJ, Kino GS, Moerner WE. Exploring the chemical enhancement for surface-enhanced Raman scattering with Au bowtie nanoantennas. J Chem Phys 2006;124:061101.
[20] Sun S, Kuang-Yu Y, Chih-Ming W, et al. High-efficiency broadband anomalous reflection by gradient meta-surfaces. Nano Lett 2012;12:6223–9.
[21] Lu G, Li W, Zhang T, et al. Plasmonic-enhanced molecular fluorescence within isolated bowtie nano-apertures. ACS Nano 2012;6:1438–48.
[22] Novotny L, Hulst N. Antennas for light. Nat Photon 2011;5:83–90.
[23] Ding L, Qin J, Guo S, Liu T, Kinzel E, Wang L. Resonant effects in nanoscale bowtie apertures. Sci Rep 2016;6:27254.
[24] Jin EX, Xu X. Obtaining super resolution light spot using surface plasmon assisted sharp ridge nano aperture. Appl Phys Lett 2005;86:111106.
[25] Buyanova IA, Chen WM. Physics and applications of dilute nitrides. New York, USA, Taylor & Francis, 2004.
[26] Henini M. Dilute nitride semiconductors: physics and technology. Oxford, Elsevier, 2005.
[27] Ayse E. Dilute III-V nitride semiconductors and material systems. Berlin, Germany, Springer, 2008.
[28] Polimeni A, Baldassarri Hoeger von Hoegersthal G, Bissiri M, et al. Effect of hydrogen on the electronic properties of $In_xGa_{1-x}As_{1-y}N_y$/GaAs quantum wells. Phys Rev B 2001;63:201304.
[29] Masia F, Pettinari G, Polimeni A, et al. Interaction between conduction band edge and nitrogen states probed by carrier effective-mass measurements in $GaAs_{1-x}N_x$. Phys Rev B 2006;73:073201.
[30] Pettinari G, Polimeni A, Masia F, et al. Electron mass in dilute nitrides and its anomalous dependence on hydrostatic pressure. Phys Rev Lett 2007;98:146402.
[31] Pettinari G, Masia F, Polimeni A, et al. Influence of nitrogen-cluster states on the gyromagnetic factor of electrons in $GaAs_{1-x}N_x$. Phys Rev B 2006;74:245202.
[32] Trotta R, Polimeni A, Capizzi M. Hydrogen incorporation in III-N-V semiconductors: from macroscopic to nanometer control of the materials' physical properties. Adv Funct Mater 2012;22:1782–801.
[33] Pettinari G, Felici M, Trotta R, et al. Hydrogen effects in dilute III-N-V alloys: from defect engineering to nanostructuring. J Appl Phys 2014;115:012011.
[34] Trotta R, Polimeni A, Martelli F, et al. Fabrication of site-controlled quantum dots by spatially selective incorporation of hydrogen in Ga(AsN)/GaAs heterostructures. Adv Mater 2011;23:2706–10.
[35] Balakrishnan N, Pettinari G, Makarovsky O, et al. Band-gap profiling by laser writing of hydrogen-containing III-N-Vs. Phys Rev B 2012;86:155307.
[36] Biccari F, Boschetti A, Pettinari G, et al. Site-controlled single-photon emitters fabricated by near-field illumination. Adv Mater 2018;30:1705450.
[37] Pettinari G, Gerardino A, Businaro L, et al. A lithographic approach for quantum dot-photonic crystal nanocavity coupling in dilute nitrides. Microelectron Eng 2017;174:16–9.
[38] Pettinari G, Felici M, Biccari F, Capizzi M, Polimeni A. Site-controlled quantum emitters in dilute nitrides and their integration in photonic crystal cavities. Photonics 2018;5:10.
[39] Bethe H. Theory of diffraction by small holes. Phys Rev 1977;66:163.
[40] Aspnes DE, Kelso SM, Logan RA, Bhat R. Optical properties of $Al_xGa_{1-x}As$. J Appl Phys 1986;60;754–67.
[41] Johnson PB, Christy RW. Optical constants of the noble metals. Phys Rev B 2012;86:155307.
[42] Guo H, Meyrath TP, Zentgraf T, et al. Optical resonances of bowtie slot antennas and their geometry and material dependence. Optics Express 2008;16:7756–66.
[43] Park S, Hahn JW, Lee JY. Doubly resonant metallic nanostructure for high conversion efficiency of second harmonic generation. Optics Express 2012;20:4856–70.
[44] Guo R, Kinzel EC, Li Y, Uppuluri SM, Raman A, Xu X. Three-dimensional mapping of optical near field of a nanoscale bowtie antenna. Optics Express 2010;18:4961–71.
[45] Wang L, Xu X. Spectral resonance of nanoscale bowtie apertures in visible wavelength. Appl Phys A 2007;89:293–7.
[46] Theiss J, Pavaskar P, Echternach PM, Muller RE, Cronin SB. Plasmonic nanoparticle arrays with nanometer separation for high-performance SERS substrates. Nano Lett 2010;10:2749–54.
[47] Fan JA, Wu C, Bao K, et al. Self-assembled plasmonic nanoparticle clusters. Science 2010;328:1135–8.
[48] Zhu W, Banaee MG, Wang D, Chu Y, Crozier KB. Lithographically fabricated optical antennas with gaps well below 10 nm. Small 2011;7:1761–6.
[49] Zehtabi-Oskuie A, Zinck AA, Gelfand RM, Gordon R. Template stripped double nanohole in a gold film for nano-optical tweezers. Nanotechnology 2014;25:495301.
[50] Chen X, Ciraci C, Smith DR, Oh SH. Nanogap-enhanced infrared spectroscopy with template-stripped wafer-scale arrays of buried plasmonic cavities. Nano Lett 2015;15:107–13.
[51] Im H, Bantz KC, Lindquist NC, Haynes CL, Oh SH. Vertically oriented sub-10-nm plasmonic nanogap arrays. Nano Lett 2010;10:2231–336.
[52] Melli M, Polyakov A, Gargas D, et al. Reaching the theoretical resonance quality factor limit in coaxial plasmonic nanoresonators fabricated by helium ion lithography. Nano Lett 2013;13:2687.
[53] Scholder O, Jefimovs K, Shorubalko I, Hafner C, Sennhauser U, Bona GL. Helium focused ion beam fabricated plasmonic antennas with sub-5 nm gaps. Nanotechnology 2013;24:395301.
[54] Wang Y, Abb M, Boden SA, Aizpurua J, de Groot CH, Muskens OL. Ultrafast nonlinear control of progressively loaded, single plasmonic nanoantennas fabricated using helium ion milling. Nano Lett 2013;13:5647–53.
[55] Kollmann H, Piao X, Esmann M, et al. Toward plasmonics with nanometer precision: nonlinear optics of helium-ion milled gold nanoantennas. Nano Lett 2014;14:4778–84.
[56] Huang I-C, Holzgrafe J, Jensen RA, Choy JT, Bawendi MG, Lončar M. 10nm gap bowtie plasmonic apertures fabricated by modified lift-off process. Appl Phys Lett 2016;109:133105.
[57] Yang H, Jin A, Luo Q, Li J, Gua C, Cui Z. Electron beam lithography of HSQ/PMMA bilayer resists for negative tone lift-off process. Microelectron Eng 2008;85:814–7.
[58] Rommel M, Weis J. Hydrogen silsesquioxane bilayer resists – combining high resolution electron beam lithography and

gentle resist removal. J Vac Sci Technol B 2013;31:06F102; and references therein.
[59] Englund D, Faraon A, Fushman I, Stoltz N, Petroff P, Vučković J. Controlling cavity reflectivity with a single quantum dot. Nature 2007;450:857–61.
[60] Galli M, Portalupi SL, Belotti M, Andreani LC, Faolain LO, Krauss TF. Light scattering and Fano resonances in high-Q photonic crystal nanocavities. Appl Phys Lett 2009;94:071101.
[61] Wang H, Goodrich GP, Tam F, Oubre C, Nordlander P, Halas NJ. Controlled texturing modifies the surface topography and plasmonic properties of Au nanoshells. J Phys Chem B 2005;109:11083–7.
[62] Rodríguez-Fernández J, Funston AM, Perez-Juste J, Álvarez-Puebla RA, Liz-Marzán LM, Mulvaney P. The effect of surface roughness on the plasmonic response of individual sub-micron gold sphere. Phys Chem Chem Phys 2009;11:5909–14.
[63] Lyamkina A, Schraml K, Regler A, et al. Monolithically integrated single quantum dots coupled to bowtie nanoantennas. Optics Express 2016;24:28936–44.
[64] Chou Chau Y-F, Chou Chao C-T, Rao J-Y, et al. Tunable optical performances on a periodic array of plasmonic bowtie nanoantennas with hollow cavities. Nanoscale Res Lett 2016;11:411.